DESIGN AND ANALYSIS OF THE SPACECRAFT COMPOSITE PAYLOAD ADAPTER WITH LOCAL SUPPORTS

Evgeny V. Morozov[1], Alexander V. Lopatin[2,3] and Alexander V. Shatov[2]

[1]School of Engineering and Information Technology, University of New South Wales at the Australian Defence Force Academy, Canberra, Australia, e.morozov@adfa.edu.au
[2]Department of Aerospace Engineering, Siberian State University of Science and Technology, Krasnoyarsk, Russia, lopatin@krasmail.ru
[3]Institute of Computational Technologies, Siberian branch of Russian Academy of Sciences, Krasnoyarsk, Russia

Keywords: Payload adapter, FEM, Buckling, Vibrations

ABSTRACT

Payload adapters are the structural elements that provide mechanical interface between spacecraft and a launch vehicle (carrier rocket). In this work, new designs of the composite adapters are proposed and analysed. The adapters are made of a carbon fabric/epoxy composite material in the form of truncated conical or polyhedral shells. In these designs, the shells of the adapters have cut-outs. The adapters do not have a bottom stiffening ring and are jointed to a launch vehicle at a number of supports. The finite-element models of the adapters were created in MSC Nastran. The buckling analyses were performed for the adapters subjected to axial compressive load and bending moment. The effects of the shell thickness and size of the cut-outs on the critical loads have been investigated. The fundamental axial and transverse vibration frequencies have been calculated for the adapters with the payload attached. These characteristics are used to assess the axial and transverse stiffness of the adapter. The effects of the shell thickness and the size of the cut-outs on the fundamental frequency have been investigated.

1 INTRODUCTION

Spacecraft that are designed to be injected into an orbit by a launch vehicle have different shapes and dimensions. To cater for these differences, the attachment of the spacecraft or satellite to the rocket launcher structure is normally performed through an adapter. There are various designs of the space adapters [1-3]. Some of the most commonly used designs are shown in Fig. 1. These include the frame-based design (see Fig. 1a), conical shell (see Fig. 1b), and conical lattice structure (see Fig. 1c).

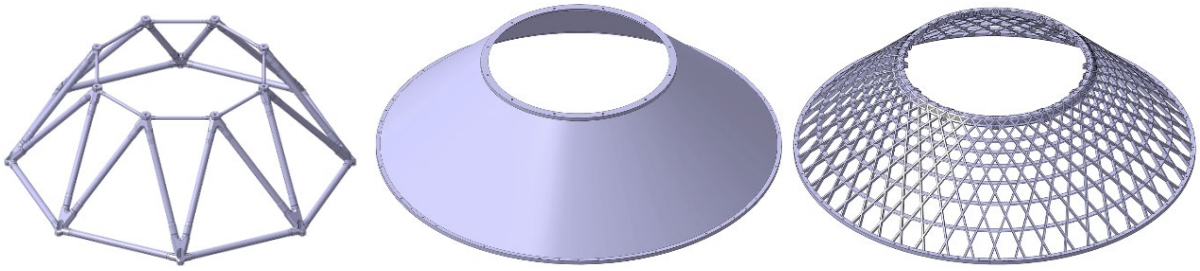

(a) (b) (c)

Figure 1: Designs of the spacecraft adapters.

Major loadings are applied to the adapter structure during the injection of the payload into an orbit. The intensity of these loadings depends on the mass of the payload and the longitudinal and transverse g-forces. To withstand these loads the adapter should have an appropriate stiffness with the minimal mass. These requirements call for new efficient designs of the adapters to be developed. In this work, a number of new adapter designs are proposed and analysed. Using finite-element models, effects of geometry parameters on the critical buckling forces and moments, and frequencies of axial and transverse vibrations are investigated.

2 ADAPTER GEOMETRY AND DESIGN

The adapters considered in this work are made of a carbon fabric/epoxy composite material in the form of truncated conical or polyhedral shells as shown in Fig. 2. In these designs, the adapters do not have a bottom stiffening ring and are jointed to a launch vehicle at several supports. The adapters have cut-outs made between the points of support (see Fig.2). The shells are assembled of trapezoid-shaped segments of a carbon fabric/epoxy prepreg and cured using vacuum bagging process. The top stiffening rings (see Fig. 3) are designed to accommodate the payload that is attached to the adapter. At the bottom, the adapter is jointed to the launcher structure through the fittings shown in Fig. 3. The spacecraft installed on the rocket launcher is shown in Fig. 4.

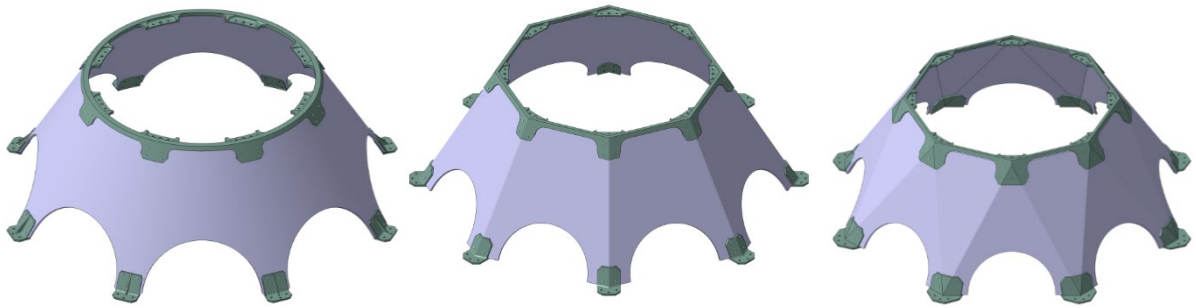

(a) (b) (c)

Figure 2: Adapter designs: (a) truncated conical shell; (b) truncated octagonal pyramid with trapezoid facets; (c) truncated octagonal pyramid with triangular facets.

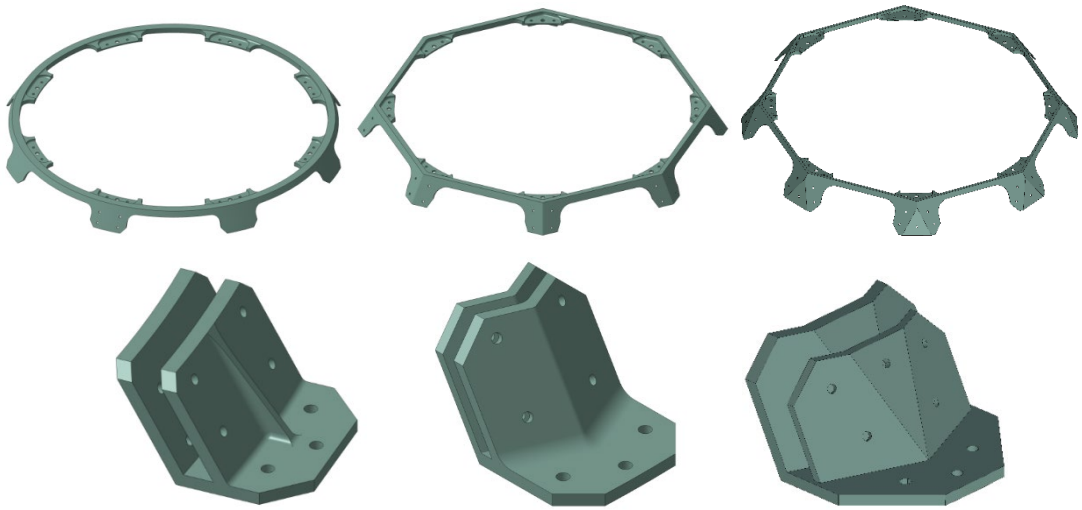

Figure 3: Top stiffening rings and bottom fittings.

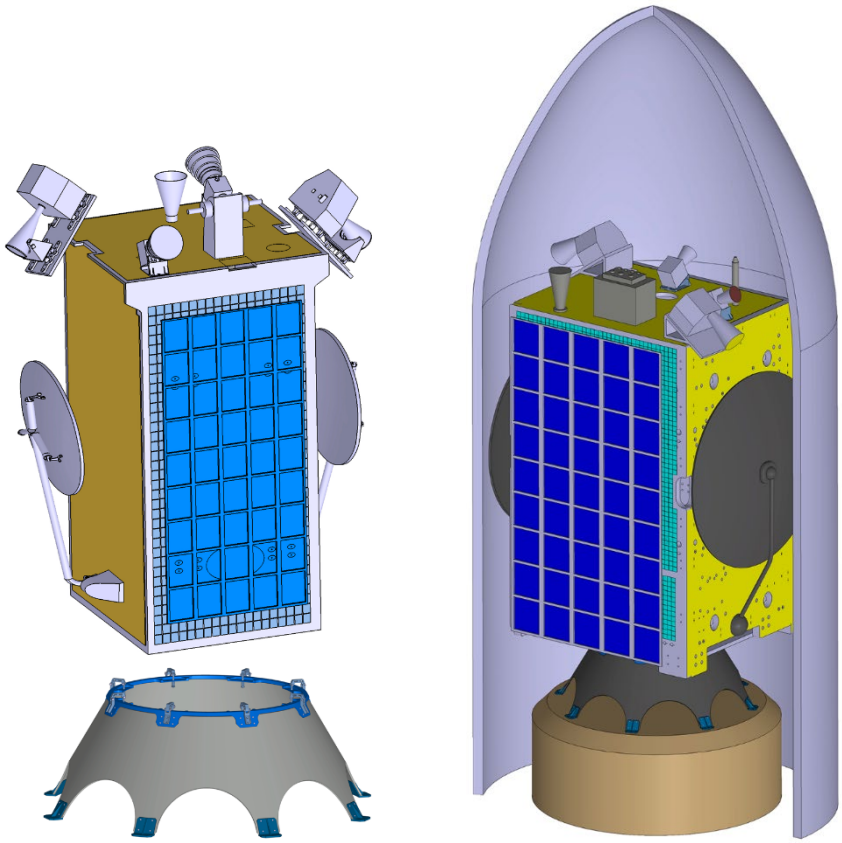

Figure 4: Spacecraft assembly.

The adapter structures shown in Fig. 2 have a number of advantages in comparison with conventional designs presented in Fig. 1. This is due to cut-outs made at the bottom. The top rings do not have high bending stiffness because of mass limitations. As a result, the local loads transmitted from the payload to such a ring cause a non-uniform distribution of internal forces in the adapter structure. Removal of the areas with the minimal internal forces using the cut-outs leads to mass reduction and more efficient utilisation of the material in the load transmission from the payload to the launcher structure. Also, the presence of cut-outs facilitates an access to the internal space of the adapter, which can be used for the installation of additional equipment.

3 FINITE-ELEMENT MODELS

The finite-element models of the adapters were created using four-node *Laminate* elements available in MSC Nastran [4]. The top base ring was meshed by the *Rigid* elements. The *Mass* elements were employed to model the payload. The input geometry parameters for the generation of finite-element models include: the height of adapter, H; diameters of the top and bottom sections D_1 and D_2, respectively; depth of the cut-out L (the shape of the cut-out is determined using spline approximation). The corresponding finite-element models of the adapters under consideration are shown in Fig. 5.

4 BUCKLING AND VIBRATION ANALYSES

As indicated earlier, the main loadings are exerted on the adapter at the orbital injection leg. The intensity of these loads is determined by a mass of the payload and maximum values of the axial and transverse g-loads. In this work, finite-element buckling analyses were performed for the adapters subjected to axial compressive load and bending moment.

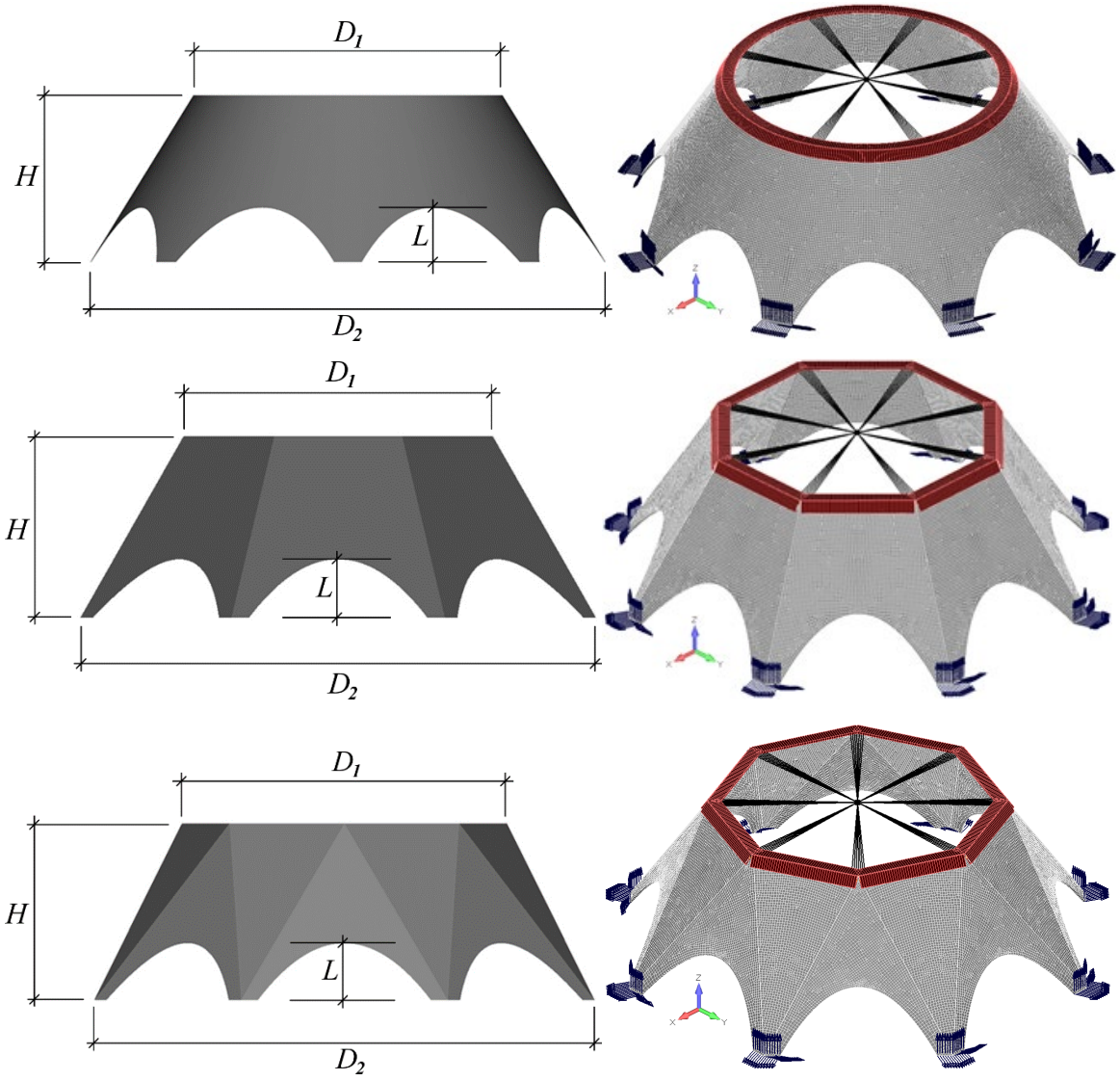

Figure 5: Finite-element models of the adapters.

The diameters of the top, D_1 and bottom, D_2 bases of the shells are 1.2 and 2 m, respectively, and the height, H is 0.65 m. The carbon fiber reinforced plastic has the following characteristics: $E_1 = 70$ GPa, $E_2 = 70$ GPa, $G_{12} = 5$ GPa, $\nu_{12} = 0.31$, $\nu_{21} = 0.31$, $\rho = 1550$ kg/m^3.

h, mm	L=150 mm	L=200 mm	L=250 mm	L=300 mm	L=350 mm	L=400 mm
5	1039.5	849.4	693.5	566.3	460.6	366.7
6	1620.2	1327.4	1081.3	878.2	709.4	561.3
7	2302.9	1951.4	1585.9	1282.2	1030.4	811.6
8	3047.2	2700.9	2219.8	1787.7	1431.1	1123.6
9	3912.6	3464.3	2994.7	2404.3	1919.1	1503.2
10	4912.2	4336.2	3840.4	3140.9	2501.7	1956.2

Table 1: Critical axial loads (kN) for the adapters in the form of conical shell.

The effects of the shell thickness, h and depth of the cut-outs, L on the critical loads have been investigated. The thicknesses of the shells were varied from 5 to 10 mm. The depth of the cut-outs ranged from 150 to 400 mm. For each combination of these structural parameters, the critical values of axial load and bending moment have been found. The values of critical axial load are presented in Tables 1, 2, and 3. The typical buckling mode shapes of the adapters under axial compression are shown in Fig. 6.

h, mm	L=150 mm	L=200 mm	L=250 mm	L=300 mm	L=350 mm	L=400 mm
5	365.8	361.1	362.3	370.9	388.1	416.3
6	625.9	617.3	618.8	632.3	659.6	705.4
7	983.6	969.3	970.4	989.3	1028.6	1095.2
8	1452.9	1430.5	1430.1	1454.4	1506.7	1596.4
9	2047.7	2014.3	2010.9	2040.1	2105.8	2220.1
10	2782.0	2734.2	2725.7	2759.1	2838.3	2977.9

Table 2: Critical axial loads (kN) for the adapters in the form of truncated octagonal pyramid with trapezoid facets.

h	L=150 mm	L=200 mm	L=250 mm	L=300 mm	L=350 mm	L=400 mm
5 mm	1231.4	1205.3	1236.5	1303.6	1135.7	700.2
6 mm	1958.2	1893.0	1902.8	1959.3	1520.0	974.3
7 mm	2910.6	2780.3	2757.5	2790.1	1934.0	1285.6
8 mm	4117.4	3897.6	3821.6	3529.4	2390.3	1638.2
9 mm	5606.8	5270.1	5120.4	4208.8	2896.5	2036.7
10 mm	7313.5	6922.2	6675.7	4948.8	3459.4	2486.0

Table 3: Critical axial loads (kN) for the adapters in the form of truncated octagonal pyramid with triangular facets.

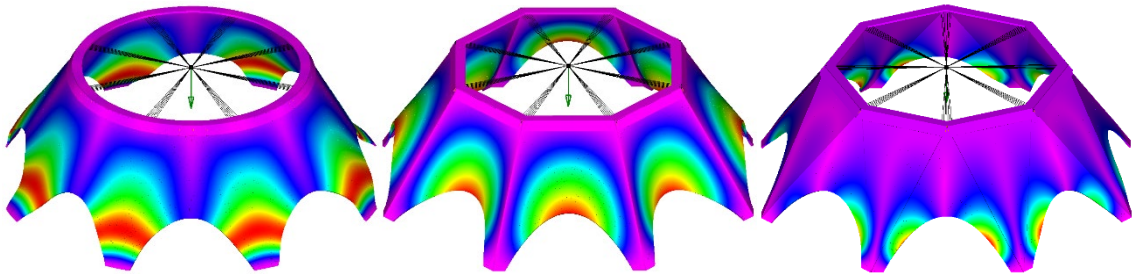

Figure 6: Typical buckling mode shapes of the adapters under axial compression.

The values of the critical buckling bending moments are presented in Tables 4, 5, and 6. Typical buckling mode shapes of the adapters under bending moment are shown in Fig. 7.

h, mm	*L*=150 mm	*L*=200 mm	*L*=250 mm	*L*=300 mm	*L*=350 mm	*L*=400 mm
5	505.2	423.4	350.8	287.5	232.9	184.6
6	789.9	655.1	538.8	440.3	355.3	280.3
7	1150.4	952.2	780.5	636.6	511.7	402.6
8	1559.3	1318.6	1081.8	881.3	705.9	554.2
9	2011.4	1737.7	1448.1	1179.4	941.2	738.3
10	2530.8	2190.8	1880.9	1533.9	1221.2	957.6

Table 4: Critical bending moments (kN · m) for the adapters in the form of conical shell.

h, mm	*L*=150 mm	*L*=200 mm	*L*=250 mm	*L*=300 mm	*L*=350 mm	*L*=400 mm
5	191.5	185.2	174.7	162.6	151.2	141.1
6	327.8	317.2	299.3	278.5	258.7	240.9
7	515.1	498.9	470.9	437.9	406.3	377.7
8	760.6	737.6	696.4	647.1	599.4	555.9
9	1071.3	1039.5	982.1	911.7	842.9	779.9
10	1454.3	1412.3	1334.4	1237.1	1141.7	1053.8

Table 5: Critical bending moments (kN · m) for the adapters in the form of truncated octagonal pyramid with trapezoid facets.

h	*L*=150 mm	*L*=200 mm	*L*=250 mm	*L*=300 mm	*L*=350 mm	*L*=400 mm
5 mm	482.3	480.0	484.5	489.7	397.4	264.6
6 mm	810.5	775.5	762.3	716.34	542.7	369.8
7 mm	1215.0	1154.5	1111.0	954.9	709.5	493.8
8 mm	1709.9	1610.1	1485.5	1220.7	900.7	638.6
9 mm	2298.7	2132.3	1895.5	1517.8	1119.0	806.4
10 mm	2984.7	2721.1	2349.9	1849.8	1367.2	999.6

Table 6: Critical bending moments (kN · m) for the adapters in the form of truncated octagonal pyramid with triangular facets.

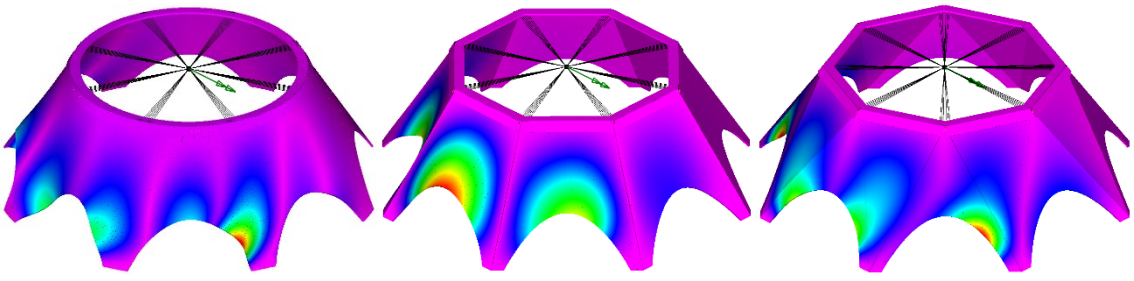

Figure 7: The typical buckling mode shapes of the adapters under bending moment.

In addition to buckling analyses. the fundamental axial and transverse vibration frequencies have been calculated for the adapters with the payload attached. The payload mass was 3000 kg with the center of mass located at 2 m from the top base of the adapter. These characteristics are used to assess the axial and transverse stiffness of the adapter. The effects of the shell thickness and the size of the cut-outs on the fundamental frequency have been investigated using the finite-element analyses. The fundamental frequencies of axial vibrations are presented in Tables 7, 8, and 9. Typical axial vibration mode shapes are shown in Fig. 8.

h, mm	*L*=150 mm	*L*=200 mm	*L*=250 mm	*L*=300 mm	*L*=350 mm	*L*=400 mm
5	75.4	74.5	73. 4	72.2	70.8	69.2
6	83.2	82.1	80.8	79.3	77.6	75.9
7	90.2	88.9	87.5	85.8	83.9	81.9
8	96.8	95.4	93.7	91.8	89.8	87.6
9	102.9	101.4	99.6	97.5	95.2	92.9
10	108.8	107.1	105.1	102.8	100.4	97.9

Table 7: Fundamental frequencies of axial vibrations (Hz) for the adapters in the form of conical shell.

h, mm	*L*=150 mm	*L*=200 mm	*L*=250 mm	*L*=300 mm	*L*=350 mm	*L*=400 mm
5	61.8	63.9	67.2	72.1	70.9	68.7
6	73.7	76.1	79.9	79.9	77.5	75.1
7	85.4	88.1	88.6	86.1	83.5	80.9
8	96.9	96.9	94.5	91.8	89.1	86.4
9	104.9	102.6	100.1	97.3	94.4	91.5
10	110.7	107.9	105.3	102.4	99.3	96.3

Table 8: Fundamental frequencies of axial vibrations (Hz) for the adapters in the form of truncated octagonal pyramid with trapezoid facets.

h, mm	*L*=150 mm	*L*=200 mm	*L*=250 mm	*L*=300 mm	*L*=350 mm	*L*=400 mm
5	78.0	76.1	73.9	71.3	68.4	64.8
6	85.2	83.2	80.8	78.0	74.8	70.9
7	91.8	89.7	87.1	84.1	80.6	76.6
8	97.9	95.7	93.0	89.8	86.2	81.9
9	103.7	101.3	98.5	95.2	91.3	86.9
10	109.2	106.7	103.7	100.3	96.3	91.7

Table 9: Fundamental frequencies of axial vibrations (Hz) for the adapters in the form of truncated octagonal pyramid with triangular facets.

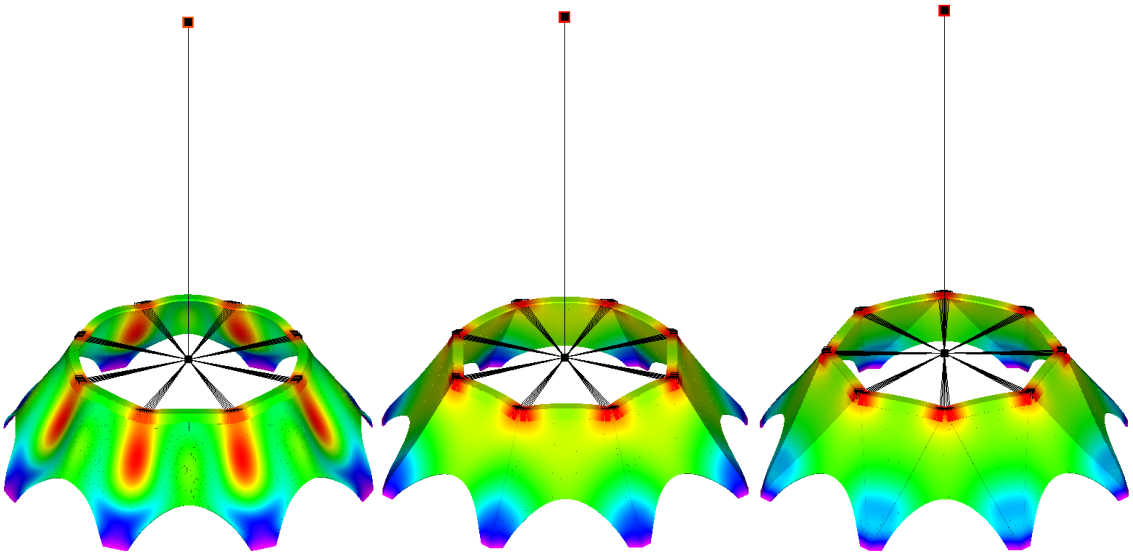

Figure 8: The typical axial vibration mode shapes of the adapters.

The fundamental frequencies of transverse vibrations are presented in Tables 10, 11, and 12. Typical transverse vibration mode shapes are shown in Fig. 9.

h, mm	*L*=150 mm	*L*=200 mm	*L*=250 mm	*L*=300 mm	*L*=350 mm	*L*=400 mm
5	16.5	16.1	15.6	15.1	14.5	13.9
6	18.4	17.9	17.4	16.8	16.1	15.6
7	20.1	19.6	19.1	18.4	17.7	16.9
8	21.6	21.1	20.5	19.8	19.1	18.3
9	23.1	22.5	21.9	21.2	20.4	19.6
10	24.4	23.9	23.2	22.5	21.7	20.7

Table 10: Fundamental frequencies of transverse vibrations (Hz) for the adapters in the form of conical shell.

h, mm	*L*=150 mm	*L*=200 mm	*L*=250 mm	*L*=300 mm	*L*=350 mm	*L*=400 mm
5	17.6	17.1	16.5	15.9	15.1	14.3
6	19.2	18.7	18.1	17.3	16.5	15.7
7	20.7	20.1	19.4	18.7	17.8	16.9
8	22.1	21.4	20.7	19.9	19.1	18.1
9	23.4	22.7	21.9	21.1	20.1	19.1
10	24.6	23.9	23.1	22.2	21.2	20.1

Table 11: Fundamental frequencies of transverse vibrations (Hz) for the adapters in the form of truncated octagonal pyramid with trapezoid facets.

h	*L*=150 mm	*L*=200 mm	*L*=250 mm	*L*=300 mm	*L*=350 mm	*L*=400 mm
5 mm	16.1	15.7	15.3	14.8	14.1	13.3
6 mm	17.8	17.4	16.9	16.4	15.6	14.7
7 mm	19.4	19.0	18.5	17.8	17.0	16.0
8 mm	20.9	20.4	19.9	19.1	18.3	17.2
9 mm	22.3	21.8	21.2	20.4	19.5	18.3
10 mm	23.6	23.0	22.4	21.6	20.6	19.4

Table 12: Fundamental frequencies of transverse vibrations (Hz) for the adapters in the form of truncated octagonal pyramid with triangular facets.

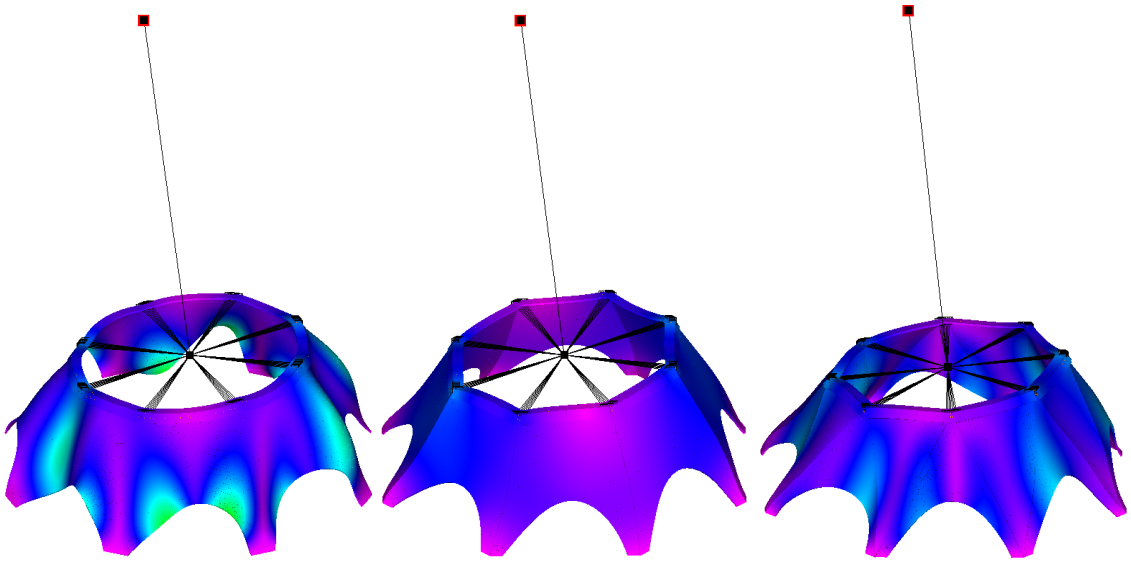

Figure 9: The typical transverse vibration mode shapes of the adapters.

CONCLUSIONS

In this work, new designs of the composite adapters are proposed and analysed. The adapters are made of a carbon fabric/epoxy composite material in the form of truncated conical or polyhedral shells. In these designs, the shells of the adapters have cut-outs. The adapters do not have a bottom stiffening ring and are jointed to a launch vehicle at a number of supports.

The finite-element models of the adapters were created in MSC Nastran. The finite-element buckling analyses were performed for the adapters subjected to axial compressive load and bending moment. The fundamental axial and transverse vibration frequencies have been calculated for the adapters with the payload attached. The effects of the shell thickness and the size of the cut-outs on the critical loads and on the fundamental frequencies were investigated.

The computational results showed that the designs of the adapters proposed in this work have considerable stiffness and can be considered as prospective structural elements. The finite-element models created for the structures under consideration allow the design analyses to be performed. Based on these analyses, the structural parameters of the adapters can be determined considering design requirements and constraints related to the stiffness and structural stability.

ACKNOWLEDGEMENTS

One of the authors (A.V. Lopatin) acknowledges the support provided by the Ministry of Education and Science of the Russian Federation (Grant ID RFMEFI57517X0144).

REFERENCES

[1] Falcon 9. Launch Vehicle Payload User's Guide. Rev. 2. 2015. http://www.spacex.com/sites/spacex/

[2] Airbus Defense and Space. Demonstrator of Carbon Anisogrid Payload Adapter. Final Presentation. 2016. https://tect.prox.esa.int/Videos/ID0020/Video/Default.html

[3] Ariane 5. User's Manual. Issue 5. Rev. 2. 2016. http://www.arianespace.com/wp-content/uploads/2011/07/Ariane5_Users-Manual_October 2016.pdf

[4] MSC Nastran. Quick reference guide's: MSC. Software Corporation; 2011